

# Simulating the Reliability of Radio Links during Superior Solar Conjunctions

A. J. Stocker<sup>1</sup>, A. Argyriou<sup>2</sup>, A. Giorgetti<sup>3</sup>, E. Paolini<sup>3</sup>, D. R. Siddle<sup>1</sup>, P. Tortora<sup>4</sup>, A. Zeqaj<sup>4</sup>, J. De Vicente<sup>5</sup>, R. Abello<sup>5</sup>, and M. Micolino<sup>5</sup>

<sup>1</sup> Department of Engineering, University of Leicester, Leicester, United Kingdom, sto@leicester.ac.uk

<sup>2</sup> Department of Electrical & Computer Engineering, University of Thessaly, Volos, Greece

<sup>3</sup> Department of Electrical, Electronic and Information Engineering, University of Bologna, Cesena, Italy

<sup>4</sup> Department of Industrial Engineering, University of Bologna, Forli, Italy

<sup>5</sup> European Space Operations Center, European Space Agency, Darmstadt, Germany

**Abstract**—Some results so far achieved in the framework of the HELIOS (Highly rEliable Links during sOlar conjunctionS) Project, funded by the European Space Agency (ESA), are presented. The purpose of the project is the definition of a TT&C communication subsystem architecture (including both ground and space segments, as well as operational methods) being robust to impairments due to superior solar conjunction, especially when the Sun-Earth-Probe angle is below 5 degrees.

**Index Terms**— Channel measurements, channel modeling, deep space communications, error correcting codes, scintillation, solar plasma, propagation.

## I. INTRODUCTION

Reliability of telemetry (TM) and telecommand (TC) communication links has always represented a main target in deep space missions [1]-[2], [4]-[5]. When a spacecraft is near superior solar conjunction, the solar plasma content in the telemetry, tracking and command (TT&C) link increases as the Sun-Earth-Probe (SEP) angle  $\beta$  gets smaller, resulting in an increased degradation of the radio signal due to amplitude and phase scintillation.

Standard deep space TT&C links exploit phase modulation techniques and are not designed for solar conjunction scenarios. As a consequence, link interruptions or complete disruptions at very low SEP angles (e.g.  $\beta < 1^\circ \div 2^\circ$  in X-band) may therefore be experienced for days or even weeks. These effects drive deep space mission design, resulting in requirements imposing no maneuvering, TC or TM at low SEP angles (e.g.,  $\beta < 5^\circ$  for maneuvering and  $\beta < 3^\circ$  for communications with ground in the case of Bepi Colombo). The operational impact of superior solar conjunctions may be significant, depending upon the orbit and level of solar activity, with severe limitations in terms of spacecraft command capabilities as well as science data returns.

The scope of this paper is to present some of the results achieved during the project aimed at defining guidelines for the ground operation during solar conjunctions.

## II. CHANNEL MODEL AND SIMULATOR

The study has been carried out by developing a software tool capable of accurately simulating the effects of solar plasma on the wireless signal for different tracking geometries, thus

enabling simulation of a complete communication chain from ground to spacecraft and back. The signal model is:

$$s(t) = \sqrt{2P_s}V(t)\sin(2\pi f_c t + \varphi_d(t) + \varphi_0 + \varphi_r(t)) + n(t) \quad (1)$$

where  $f_c$  is the carrier frequency,  $P_s$  is the total average signal power,  $V(t)$  is the fading amplitude due to scintillation,  $\varphi_r(t)$  is the phase scintillation term,  $\varphi_0$  is an arbitrary, constant phase,  $\varphi_d(t)$  is the phase modulated data and  $n(t)$  is additive white Gaussian noise (AWGN) with one-sided Power Spectral Density (PSD)  $N_0$  (watt/Hz).

The channel model, for a one-way link between two participants, is broadly defined as:

$$h(t) = A(t)e^{j\theta(t)} \quad (2)$$

where:

- $A(t)$  is the amplitude term;
- $\theta(t)$  is the channel phase term.

Both of these terms include the scintillation that is derived from open-loop data from the ESA Mars Express mission during its 2013 superior solar conjunction. The amplitude scintillation and phase scintillation were each characterized separately before being recombined in the simulator.

The software simulator, considering the equivalent base-band system, is based on the Monte Carlo method where each run corresponds to the transmission of a single block/frame of bits and different channel realizations that are provided by the channel model. The simulation of multiple frames ensures that bit error rate (BER) and frame error rate (FER) are statistically valid.

## III. PLASMA NOISE AND PLL

There is a clear dependence of the phase variance on the bandwidth of the Phase Lock Loop (PLL), which should be small to maximize the carrier loop Signal-to-Noise Ratio (SNR), but large enough to track static phase error due to Doppler dynamics, and the contribution to carrier loop

phase error variance due to phase noise (e.g. a result of solar coronal effects) on the link.

#### IV. ANALYTICAL EQUATIONS FOR SOLAR PHASE NOISE VARIANCE

##### A. Basic model (without fading)

The total variance,  $\sigma_\phi^2$ , is the sum of the phase variance due to the solar coronal scintillation,  $\sigma_S^2$ , and that due to thermal noise,  $\sigma_N^2$ . The latter is inversely proportional to the signal to noise ratio in the PLL, whilst the solar variance is a more complicated function of the SEP angle and bandwidth.

An expression for  $\sigma_S^2$  is obtained by using the HELIOS channel model to produce PSDs of phase variation for a range of different values of  $\beta$  and the two-sided Loop Bandwidth ( $2B_L$ ). These are then convolved with the PLL transfer function to characterise the phase variance due to solar phase noise, which is then fitted on a log-log plot to  $\beta$  and  $2B_L$ , using a first order surface-fit, to obtain gradients and intercept. Specifically, the best-fit values of  $p$ ,  $q$  and  $r$ , are determined in the equation

$$\log_{10} \sigma_S^2 = p + q \log_{10} \beta + r \log_{10} 2B_L \quad (3)$$

The constant can be expressed as  $C = 10^P$  and then separated out as factors:  $C = C_{band} C_{pll} C_q$  which depend on band (S, X or Ka), PLL damping factor and signal quality, respectively. The quality factor is good, moderate or poor, based on the lower decile, median and upper decile of observed phase scintillation respectively. Thus, (3) can be rewritten as

$$\sigma_S^2 = \frac{C_{band} C_{pll} C_q}{\beta^q (2B_L)^r} \quad (4)$$

Moreover, the thermal variance is

$$\sigma_N^2 = \frac{0.5}{SNR_{PLL}} = \frac{2B_L}{2 SN0_{PLL}} \quad (5)$$

where  $SNR_{PLL}$  is the two-sided signal-to-noise ratio experienced by the PLL, which is related to the signal-to-noise-density ratio (SN0) in the carrier only ( $SN0_{PLL}$ ) and the PLL bandwidth. The complete model of the phase variance is therefore

$$\sigma_\phi^2 = \frac{C_{band} C_{pll} C_q}{\beta^q (2B_L)^r} + \frac{2B_L}{2 SN0_{PLL}} \quad (6)$$

Differentiating (6) and equating to zero provides us with an expression for the optimum value of  $2B_L$  (i.e. the value yielding the minimum  $\sigma_\phi^2$ ):

$$(2B_L)_{opt} = \left[ \frac{2 SN0_{PLL} C_{band} C_{pll} C_q}{\beta^q} \right]^{\frac{1}{r+1}} \quad (7)$$

Figure 1 shows how the optimum PLL bandwidth derived in (7) varies with SN0, the carrier to noise density ratio. The

point at which the total phase variance just exceeds  $0.1 \text{ rad}^2$  (the value of phase variance that, for a residual carrier, will lead to the PLL not tracking the phase), indicated in the graph where the plotted lines are dashed, occurs at larger  $2B_L$  and higher SN0 with decreasing  $\beta$ .

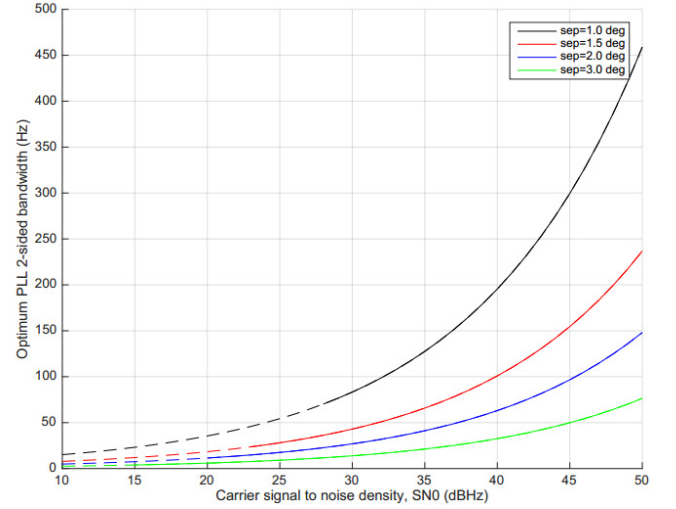


Figure 1: The optimum PLL 2-sided bandwidth,  $(2B_L)_{opt}$  for X-band uplink with an underdamped PLL as a function of CN0. Dashed lines show where  $\sigma_\phi^2$  exceeds  $0.1 \text{ rad}^2$ .

##### B. Fading model

The fading model combines fades due to amplitude scintillation with increased thermal phase noise. It is derived from the model in the preceding section by reducing the Carrier-to-Noise ratio (CN0) when an amplitude fade occurs. The model estimates the phase variance that is exceeded  $p\%$  of the time, based on the amplitude probability density distributions from thirty-two intervals of Mars Express observations in 2013. The amplitude in each interval was fitted to a Nakagami distribution, which is defined for positive values of  $x$  (here representing the received signal amplitude) using parameters  $\mu$  and  $\omega$  by:

$$N(x, \mu, \omega) = \frac{2\mu^\mu x^{2(\mu-1)}}{\omega \Gamma(\mu)} \exp\left(-\frac{\mu x^2}{\omega}\right) \quad (8)$$

Values of  $\mu$  and  $\omega$  were derived from the measurements.  $\mu$  is given as a function of SEP by eq. (9), with  $\alpha_3 = -0.0165$ ,  $\alpha_2 = 0.4156$ ,  $\alpha_1 = -3.5084$ ,  $\alpha_0 = 6.8475$ ,  $\mu_{max} = 26$  and  $\mu_{min} = 0.5$ , whereas  $\omega$  has a single value,  $3.122 \times 10^7$ .

$$\mu_{model} = \frac{\mu_{max}}{1 + \exp(\alpha_3 \beta^3 + \alpha_2 \beta^2 + \alpha_1 \beta + \alpha_0)} + \mu_{min} \quad (9)$$

Once  $\omega$  and  $\mu$  have been parametrised, a distribution of  $\sigma_\phi^2$  for any SEP angle and any fading percentile can be found from these parameters, as seen in Figure 2. The black line shows the mean value, while the other lines show the expected variance exceeded  $p\%$  of the time, where  $p = 1, 10, 50$  and  $90$ .

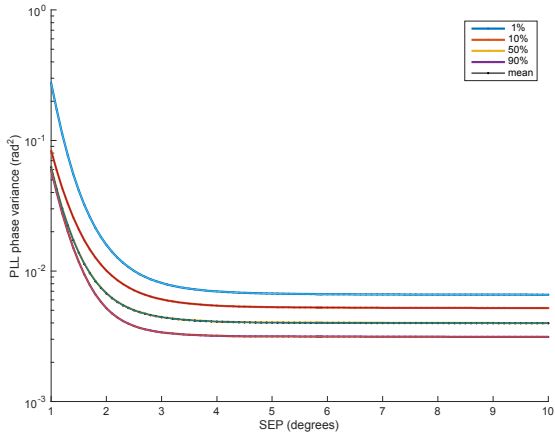


Figure 2: The PLL phase variance exceeded for various probabilities of occurrence for X-band uplink with an underdamped PLL versus SEP as generated by (6) with poor channel quality and a nominal  $CN_0 = 38$  dB Hz. Note that the median line is obscured by the mean line.

## V. SIMULATION RESULTS

We report an example for a mission to Jupiter with both Uplink and Downlink in order to show the applicability of the optimum PLL bandwidth. The radio link configurations are summarized in Table 1.

Uplink		Downlink	
Parameter	Value	Parameter	Value
Modulation	BPSK	Modulation	BPSK
S/N0	31.15 dBHz	S/N0	39.07 dBHz
Mod index	0.6 rad	Mod index	0.7 rad
Code	BCH 57/63	Code	Turbo 1/4
			8920/35680
SEP	3 deg	SEP	3 deg

Table 1: Jupiter Scenario specifications

### A. Uplink

Using the basic model, the value of the optimum PLL bandwidth is found (see Figure 3) to be 13 Hz. This is then verified using the simulator (see Figure 4).

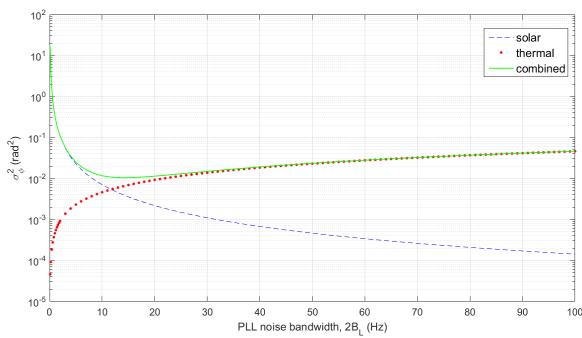


Figure 3: Phase noise vs PLL Bandwidth ( $2B_L$ ) derived from the basic model

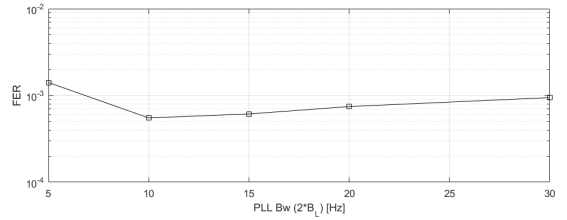


Figure 4: Frame Error Rate (FER) vs PLL Bw ( $2B_L$ ) for an  $E_b/N_0$  of 8.3 dB (simulator output).

The two results are in good agreement. Figure 5 depicts a simulation output in terms of FER vs  $E_b/N_0$  (where  $E_b$  is the energy per information bit) for the optimum PLL bandwidth.

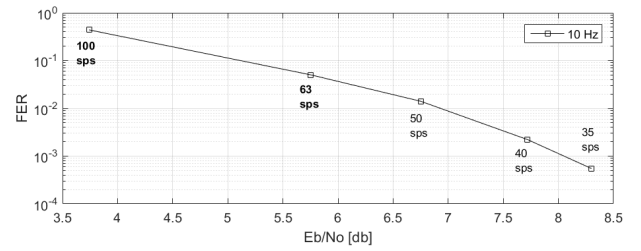


Figure 5: FER vs  $E_b/N_0$  for the optimum  $2B_L$ , (bold symbol rates are the ones actually used in uplink)

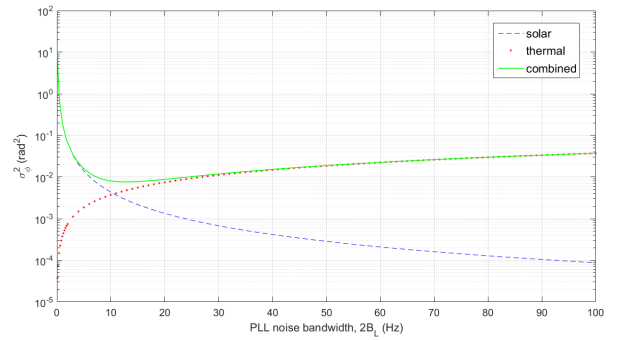


Figure 6: Phase noise vs PLL Bandwidth ( $2B_L$ ) derived from the basic model

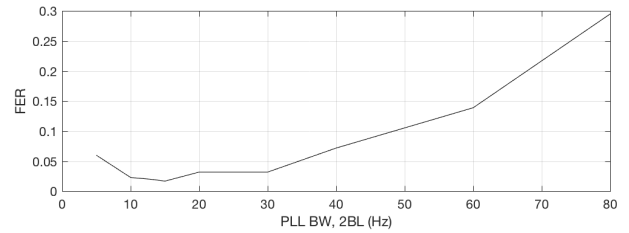


Figure 7: FER vs PLL BW,  $2B_L$  for a  $k=8920$ , 1/4 turbo code with  $E_b/N_0=0.02$  dB at  $SEP=3^\circ$ .

## B. Downlink

The same procedure is used also for the downlink case. First the optimum PLL bandwidth ( $\sim 13$  Hz) is found using the basic model (see Figure 6). This is then verified using the simulator (see Figure 7).

Then a simulation is performed with the optimum PLL bandwidth. In this scenario, we note from Figure 8 that an acceptable performance ( $FER < 10^{-5}$ ) is only achieved for a symbol rate of 500 symbols-per-second (sps) or less.

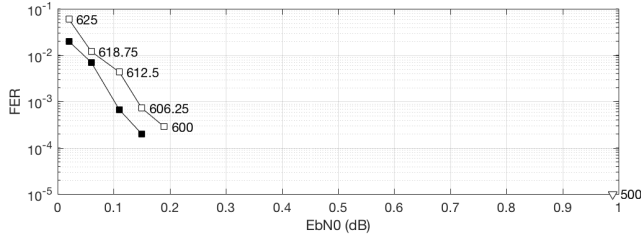


Figure 8 : FER vs  $E_b/N_0$  for two different  $2B_L$  (same configuration of Figure 7)

## VI. CONCLUSIONS AND FUTURE WORK

For  $\beta = 3^\circ$  and X-band, the amplitude scintillation index caused by the solar plasma is not too large ( $m = 0.1 \div 0.3$ ) and the largest contributor to phase variance, at bandwidths beyond a few Hz, is thermal noise rather than phase scintillation caused by the solar corona. Therefore, current technologies appear to work to a greater or lesser extent depending on  $SN_0$  and  $E_b/N_0$ . For values of SEP less than  $3^\circ$  the increasing amplitude scintillation and phase variance due to the solar corona imply that a) a PLL is unlikely to be able to reliably lock the phase and b) deep fading will make the signal no longer be detectable (in addition such deep fades can cause phase, or cycle, slips). Figure 9 illustrates the effect of introducing amplitude fading into the analytic model. For  $\beta = 3^\circ$  the fading level is sufficiently small such that even at the 1% level (i.e. only 1% of the amplitude fades are worse than this) the PLL phase variance is less than  $0.1 \text{ rad}^2$ ; in this condition the PLL would lock and a link based on a turbo code would operate at a  $FER < 10^{-5}$  provided  $E_b/N_0$  is large enough. The effect of severe fading at  $\beta = 1^\circ$  is immediately apparent (the fading depth being approximately 17 dB), with the phase variance exceeding that required to track the phase with the PLL (i.e.,  $0.1 \text{ rad}^2$ ) for somewhere between 50% and 90% of the time even close to the optimum PLL bandwidth. We note that the phase slips resulting from the deep fading caused by the solar plasma (similar to those caused by thermal noise at low SNR) are not included in the analytical model and these will further compromise the ability of the PLL to track the phase. Proposed solutions to these problems must be aimed at either reducing the level of scintillation or mitigating the effects.

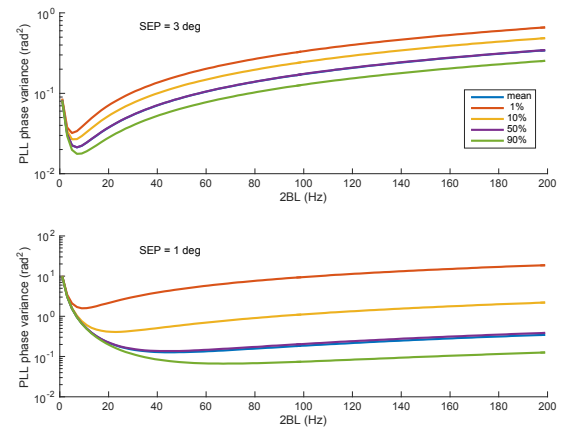


Figure 9 : PLL Phase variance at  $SEP=3^\circ$  (top panel) and  $SEP=1^\circ$  for PLL  $SN_0=25$  dB. The different lines correspond to the probability of different fading levels (i.e. 1% represents the phase variance exceeded 1% of the time).

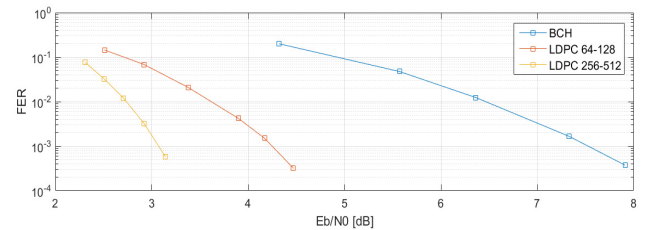


Figure 10 : FER vs  $E_b/N_0$  comparison for three different codings at  $SEP=3^\circ$  and PLL  $SN_0=44.7$  dB Hz (the specifics of the simulation are given in Table 1, Uplink case).

Further directions of investigation will include CCSDS LDPC codes for TM and TC, non-coherent demodulation and multi-frequency links, along the lines hereafter described.

### A. LDPC codes

The CCSDS recently included in its recommendation [3] nine LDPC codes, belonging to the class of accumulate-repeat-jagged-accumulate (ARJA), for deep space bandwidth efficient high data rates applications [4],[5]. The selected code rates are 1/2, 2/3, and 4/5; for each code rate and frame lengths of 1024, 4096, and 16384 bits are possible. Recently, the CCSDS selected (but have not yet standardized) two short LDPC codes for next generation TC applications, both of rate 1/2, one with frame length 64 bits and the other with frame length 256 bits [6],[7].

In order to investigate to what extent deep space missions employing CCSDS LDPC codes are affected by superior solar conjunctions, encoding and decoding algorithms (e.g., belief propagation, offset min-sum) for CCSDS LDPC codes have been implemented in the software simulator and preliminary results in presence of solar plasma have been obtained. An example for the uplink is depicted in Figure 10. The goal of this activity is evaluating robustness of current LDPC codes to solar conjunctions at different SEP

values, and, possibly, to design appropriate counter-measures.

### B. Non coherent demodulation (FSK and DBPSK)

Another interesting idea involves modulation schemes that can be decoded with non-coherent receivers that require no knowledge of the channel or estimation of the phase with a PLL. The first one is the differential BPSK signaling scheme (DBPSK). We will implement a non-coherent DBPSK receiver for this purpose. We will also investigate how additional binary signaling modulation schemes (beyond phase modulation) perform at low SEP angles. For the particular case of superior solar conjunction events, the use of FSK was proposed in the literature for spacecraft located at Mars. This means that FSK will be part of the solutions studied and investigated.

### C. Multifrequency links

Given the complexity of implementing (also in terms of on-board RF network) a full multifrequency link where not only Doppler (carrier) observables can be generated, but also real TM/TC, we'd like to pursue the idea of quantifying the advantages of having a single Ka-up/Ka-down link, as currently envisaged on-board some future missions, given the recent development of Integrated Deep Space Transponders (with integrated X-up and Ka-up + X-down and Ka-down link capabilities). Thus, instead of proposing the simulation of the full multifrequency link TT&C, we intend to expand our S/W simulator capabilities to simulate also Ka-band uplink and Ka-band downlink links, by using the existing channel model and scaling this up by using existing experimental data of scintillation index and Allan standard deviation at Ka-band at various SEP angles.

### ACKNOWLEDGMENT

The research described in this paper was carried out in the framework of ESA contract No. 4000112986/14/F/MOS "Reliable TT&C during superior solar conjunctions". The authors want to express their gratitude to the ESA personnel involved in this project for providing their precious suggestions, remarks and operational experience.

### REFERENCES

- [1] J. Massey, J. Hagenauer, "Deep-space communications and coding: A marriage made in heaven" in *Advanced Methods for Satellite and Deep Space Communications*, Heidelberg, Germany and New York:Springer, vol. 182, pp. 1-17, 1992.
- [2] T. de Cola, E. Paolini, G. Liva, and G. P. Calzolari, "Reliability options for data communications in the future deep-space missions," *Proc IEEE*, vol. 99, no. 11, pp. 2056–2074, Nov. 2011
- [3] *TM Synchronization and Channel Coding*, Recommendation for Space Data System Standards, 131.0-B-2. Blue Book, Issue 2, Consultative Committee for Space Data Systems (CCSDS), Aug. 2011
- [4] K. Andrews, D. Divsalar, S. Dolinar, J. Hamkins, C. Jones, and F. Pollara, "The development of turbo and LDPC codes for deep-space applications," *Proc. IEEE*, vol. 95, no. 11, Nov. 2007

- [5] G. P. Calzolari, M. Chiani, F. Chiaraluce, R. Garello, and E. Paolini, "Channel coding for future space missions: New requirements and trends," *Proc. IEEE*, vol. 95, no. 11, pp. 2157-2170, Nov. 2007
- [6] *Short Block Length LDPC Codes for TC Synchronization and Channel Coding*, Experimental Specification, 231.1-O-1. Orange Book, Issue 1, Consultative Committee for Space Data Systems (CCSDS), Apr. 2015
- [7] M. Baldi, *et al.*, "State-of-the-art space mission telecommand receivers," *IEEE Aerosp. Electron. Syst. Mag.*, vol. 32, no. 6, pp. 4-15, Jun. 2017